IOP Conf. Series: Materials Science and Engineering **280** (2017) 012006 doi:10.1088/1757-899X/280/1/012006

Modeling and Analysis of the Static Characteristics and Dynamic Responses of Herringbone-grooved Thrust Bearings

Yunluo Yu, Guang Pu and Kyle Jiang*

University of Birmingham, Birmingham B15 2TT, United Kingdom

*K.Jiang@bham.ac.uk

Abstract. This paper describes a theoretical investigation of static and dynamic characteristics of herringbone-grooved air thrust bearings. Firstly, Finite Difference Method (FDM) and Finite Volume Method (FVM) are used in combination to solve the non-linear Reynolds equation and to find the pressure distribution of the film and the total loading capacity of the bearing. The influence of design parameters on air film gap characteristics, including the air film thickness, depth of the groove and rotating speed, are analyzed based on the FDM model. The simulation results show that hydrostatic thrust bearings can achieve a better load capacity with less air consumption than herringbone grooved thrust bearings at low compressibility number; herringbone grooved thrust bearings can achieve a higher load capacity but with more air consumption than hydrostatic thrust bearing at high compressibility number; herringbone grooved thrust bearings would lose stability at high rotating speeds, and the stability increases with the depth of the grooves.

1. Introduction

Herringbone grooved thrust air bearings have been widely employed in high speed and light weight rotational machinery, such as small precision motors, gas expanders, spindles because of its excellent load capacity and stability compared with other types of bearings. Herringbone grooves inscribed on either a rotating or stationary machine component pump lubricating air inward to raise air film stiffness and the threshold speed of the whirling stability. The grooves can also be engraved fully or partially on a surface with a certain angle inclined to the axial direction. The large variety and complex geometries of the grooves pose challenges for the designs of herringbone grooved thrust bearings. Nevertheless, the references dealing with the effective design methodology of herringbone grooved thrust bearings are very limited when compared with the references on the bearing characteristic analysis [1]. Therefore, even though herringbone grooved thrust bearings have been applied for a long time, there is still a need in theoretical studies to predict their performances accurately.

Fundamentally, numerical analysis of herringbone grooved thrust bearings is to study the bearing performance by solving the Reynolds Equation numerically. As a second order partial differential equation, there are three discrete schemes which can be used: Finite Difference Method (FDM), Finite Element Method (FEM) and the Finite Volume Method (FVM). Florin suggested that by applying Newton's method, it can reduce computational time significantly [2]. Newton's method is also proven to have better stability in getting converged solutions [3]. Nenzi Wang carried out a series of studies on numerical methods which can be applied to solve a compressible Reynolds Equation [4-6]. The work includes comparisons of different methods with respect to computational time and stability. He also proposed various criteria to stop an iterative process and analyzed the truncation errors of

numerical approaches [4-6]. The above mentioned approaches are all based on FDM and they have good agreement with experiment results for static air bearings. The FVM is also adopted by some researchers. It is based on the continuity equation and Green's theorem. This approach shows advantages in dealing with film discontinuities and some pocket restrictor configurations [7]. In reference to the advantages of the FDM and FVM, these two methods are combined to solve the Reynolds Equation in this study.

In this paper, a numerical model for herringbone grooved thrust bearings is proposed based on the FDM and FVM; and then, the motion equations are added into the model to get the dynamic response of herringbone grooved thrust bearings; finally, the effects of several designs and working parameters on air film characteristics of herringbone grooved thrust bearings, including the air film thickness, rotating speed and groove depth, are investigated and compared with hydrostatic thrust air bearings.

2. Modeling

2.1. Reynolds equations and the finite difference scheme

In this section, a numerical model based on the FDM and FVM is developed for herringbone grooved thrust air bearings in order to study the effect of design parameters on air film characteristics, including the air film thickness, groove depth and rotating speed.

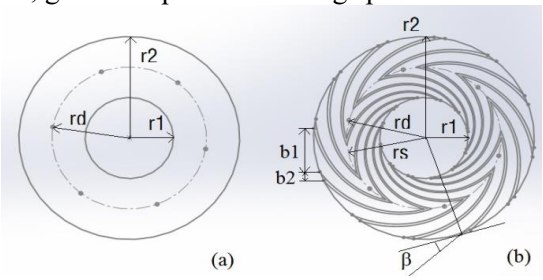

Figure 1. The geometries of (a) the hydrostatic thrust bearing and (b) the herringbone grooved thrust air bearing

The geometries of the herringbone grooved thrust air bearing studied in this paper and the hydrostatic thrust bearing which used for comparison are shown in Fig.1. In order to model arbitrarily shaped herringbone grooves of thrust bearings effectively, the coordinate system of the bearing surface can be transformed in reference to the boundaries of the grooves as shown in Fig.2.

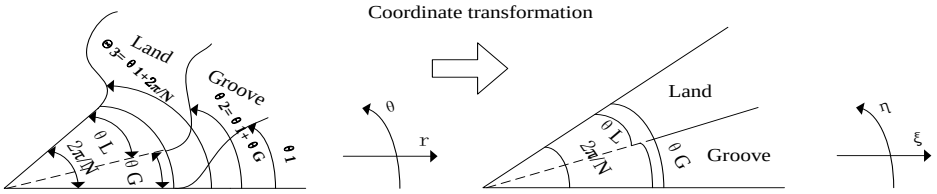

Figure 2. Bearing geometry transformation based on the boundary fitted coordinate system

The transformation functions of the coordinate system are listed as Eq.(1) and Eq.(2):

$$\xi = r \tag{1}$$

$$\begin{cases} Inner: \eta = \theta - In(r/r_s)/tan\beta \\ Outer: \eta = \theta - \left\{In\left(\frac{r_s}{r_2}\right) - In\left(\frac{r}{r_2}\right)\right\}/tan\beta \end{cases} \tag{2}$$

After introducing the dimensionless variables:

$$\zeta = \frac{\xi}{r_2}, P = \frac{p}{p_a}, H = \frac{h}{h_0}, u = \frac{\omega r_2}{2}, \tau = \omega t \tag{3}$$

where r_2 is the outer radius of the bearing, p_a the atmospheric pressure, h_0 the reference film thickness, h the film thickness, t the time. With the assumption that the isothermal perfect gas is used, the Reynolds equation of compressible flow can be written as:

$$\frac{\partial}{\partial\zeta}\left(\zeta PH^3\frac{\partial P}{\partial\zeta}\right)+\frac{1}{\zeta}\frac{\partial}{\partial\eta}\left(PH^3\frac{\partial P}{\partial\eta}\right)=\Lambda\zeta\frac{\partial(PH)}{\partial\eta}+2\Lambda\zeta\frac{\partial(PH)}{\partial\tau} \tag{4}$$

$$\Lambda=\frac{6\mu\omega r_2}{p_a{h_0}^2} \tag{5}$$

where Λ is known as the compressibility number or bearing number, μ the viscosity of the air film. To solve the Reynolds Equation, a control volume is defined as Fig.3. The mass flow rate Q^{ζ}, which across the boundary of $\zeta = constant$ and the mass flow rate Q^{η}, which across the boundary of $\eta = constant$ are, respectively, calculated as Eq.(6) and Eq.(7).

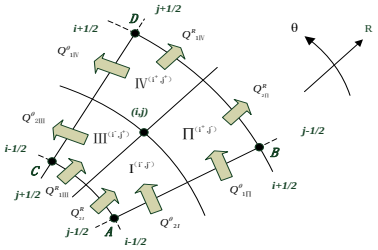

Figure 3. The defined control volume

$$Q^{\zeta}=\int_{\zeta_1}^{\zeta_2}(-\zeta PH^3\frac{\partial P}{\partial\zeta}+\Lambda\zeta PH)d\zeta \tag{6}$$

$$Q^{\eta}=\int_{\eta_1}^{\eta_2}(-PH^3\frac{\partial P}{\partial\eta})d\eta \tag{7}$$

The mass flow rate due to squeezing motion inside the control volume is expressed as follows:

$$Q^{\tau}=\int_{\eta_1}^{\eta_2}\int_{\zeta_1}^{\zeta_2}(2\Lambda\zeta\frac{\partial PH}{\partial\tau})d\zeta d\eta \tag{8}$$

The following relationship can be found from the mass flow rate balance on the control volume:

$${Q^{\eta}}_{2I}+{Q^{\eta}}_{1III}-{Q^{\eta}}_{2II}-{Q^{\eta}}_{1IV}+{Q^{\zeta}}_{2I}+{Q^{\zeta}}_{1II}-{Q^{\zeta}}_{2III}-{Q^{\zeta}}_{1IV}=Q^{\tau}+Q^{orifice} \tag{9}$$

where $Q^{orifice}$ is the mass flow rate of the orifice. The dimensionless mass flow rate of the orifice can be calculated according to the following equations under isentropic assumption:

$$Q^{orifice}=\begin{cases}HC_s\left\{\frac{2}{\gamma-1}\left[\left(\frac{P_r}{P_s}\right)^{2/\gamma}-\left(\frac{P_r}{P_s}\right)^{(\gamma+1)/\gamma}\right]\right\}^{1/2}, & if\ \ \frac{P_r}{P_s}\geq\left(\frac{2}{\gamma+1}\right)^{(\gamma-1)/\gamma}\\ HC_s\left(\frac{2}{\gamma+1}\right)^{\left(\frac{(\gamma+1)}{2(\gamma-1)}\right)}, & if\ \ \frac{P_r}{P_s}<\left(\frac{2}{\gamma+1}\right)^{(\gamma-1)/\gamma}\end{cases} \tag{10}$$

$$C_s=\frac{12\mu\pi dC_dP_s}{h_0^2p_{at}^2}\sqrt{\gamma\Re T} \tag{11}$$

where T is the atmospheric temperature at supply conditions, C_d the discharge coefficient, d the orifice diameter, μ the dynamic viscosity of the fluid, γ the isentropic index and $\Re$ the gas constant. Powel [8] regarded C_d as a function of the pressure ratio $\frac{P_r}{P_s}$. However, many researchers take the coefficient as 0.8 for all flow conditions [9]. In this study, C_d is taken as 0.8 in all the cases. By solving Eq.(1), the pressure distribution of the lubricating can be found.

2.2. Calculation of static characteristics

For a thrust bearing experiencing a small vibration in the axial direction, the minimum air film thickness and pressure can be expressed as:

$$h = h_0 + \varepsilon e^{j\omega_f t}$$
$$p = p_0 + \varepsilon p_t e^{j\omega_f t} \quad (12)$$

where ε represents the function of air film thickness and the bound of ε is approximately within ±10 percent of the steady state air film thickness. Subscripts 0 and *t* mean the physical quantities under the steady and unsteady operation conditions, respectively.

Based on the equilibrium on the control volume, the following relationships can be obtained:

$$F_0(P_0) = Q^{\eta}{}_{2I0} + Q^{\eta}{}_{1III0} - Q^{\eta}{}_{2II0} - Q^{\eta}{}_{1IV0} + Q^{\zeta}{}_{2I0} + Q^{\zeta}{}_{1II0} - Q^{\zeta}{}_{2III0} - Q^{\zeta}{}_{1IV0} - Q^{orifice} = 0 \quad (13)$$

$$F_t(P_t, P_0) = Q^{\eta}{}_{2Is} + Q^{\theta}{}_{1IIIs} - Q^{\eta}{}_{2IIs} - Q^{\eta}{}_{1IVs} + Q^{\zeta}{}_{2Is} + Q^{\zeta}{}_{1IIs} - Q^{\zeta}{}_{2IIIs} - Q^{\zeta}{}_{1IVs} - Q^{\tau}{}_{s} - Q^{orifice} = 0 \quad (14)$$

Eq. (13) is a nonlinear equation which can be solved by applying the Newton-Raphson iteration method. Eq.(14) is a linear equation which can be solved based on the steady state pressure P_0 obtained through Eq.(13).

In this work, maximization of the bearing load capacity and minimization of the consumption of compressed air are considered as the way to the optimal design of the herringbone grooved bearings. The consumption of compressed air is the air flow rate of all the orifice restrictors. The load capacity can be calculated using the following equation:

$$w = \int_{\xi_1}^{\xi_2} \int_0^{2\pi} (p_0 - p_a) \xi d\xi d\eta \quad (15)$$

2.3. Calculation of dynamic responses

The calculation requires to solve the Reynolds equation with the equation of motion [10-11] simultaneously. The Reynolds equations have been introduced in Section 2.2. The equation of motion can be written as:

$$\Delta w(t) = m\ddot{h} \quad (16)$$

where *m* is the mass supported by the bearing, Δw is the variation of the resultant pressure force. The dynamic response of thrust air bearing can be calculated using the following scheme:

1. Choose an equilibrium position of the simulated thrust bearing for dynamic calculation.
2. Input initial step displacements and velocities for step by step method.
3. Dynamic calculation of the movement (acceleration, velocity, displacement, pressure and load capacity, etc.)

3. Numerical simulation

3.1. Thrust bearings for simulation

Table 1. Specification of test bearings

Bearing Type	Specifications
Hydro-static (Type 1)	$r_1 = 6mm, r_2 = 15mm, r_d = 10.5mm,$
Herring bone (Type 2)	$r_1 = 6mm, r_2 = 15mm, r_d = 10.5mm, r_s = 10.5mm, h_g = 10\mu m, \beta = 16deg, \frac{b_1}{b_2} = 1.667 N = 24$
Herring bone (Type 3)	$r_1 = 6mm, r_2 = 15mm, r_d = 10.5mm, r_s = 10.5mm, h_g = 20\mu m, \beta = 16deg, \frac{b_1}{b_2} = 1.667, N = 24$
Herring bone (Type 4)	$r_1 = 6mm, r_2 = 15mm, r_d = 10.5mm, r_s = 10.5mm, h_g = 30\mu m, \beta =$

$$16deg, \frac{b_1}{b_2} = 1.667, N = 24$$

In this section, the herringbone grooved thrust bearing and the hydrostatic thrust air bearing shown in Fig.1 and Tab.1 are simulated using the proposed FDM and FVM model. Then, the influences of several design parameters of the thrust bearings on its characteristics have been investigated to provide information in the future design of hydrostatic thrust air bearing. The design parameters including the air film thickness, rotating speed, groove depth and external load.
Other fixed parameters are listed in Tab.2.

Table 2. Fixed parameters of bearings studied

Bearing parameters	Value	Bearing parameters	Value
Reference gap h_0(um)	20	Coefficient of discharge C_d	0.8
Radius of orifices r_d	10.5×10^{-3}	Isentropic index γ	1.4
Diameter of orifices d_0	250×10^{-6}	Gas constant $\mathcal{R}$ (J kg^{-1} K^{-1})	287
Supply pressure p_s (Pa)	6×10^{-5}	Dynamic viscosity u (Pa s)	18.38×10^{-6}
Atmospheric pressure p_{at} (Pa)	1×10^{-5}	Temperature at supply conditions T (^{o}K)	293

3.2. Analysis of static characteristics

In some applications, it is preferable to reduce air consumption while maintaining reasonable load capacity. For this reason, the influence of air film thickness, rotating speed and groove on load capacity and mass flow rate have been investigated .

When the rotor is stationary, the load capacity and mass flow rate of the thrust bearings against the air film thickness are respectively presented in Fig.4, where p_s =3×10^5 Pa, $n_{ori} = 6$ and $\omega = 0$ rpm. When the rotor speed is at 300000 rpm, the load capacity and mass flow rate of all the orifice restrictors against the air film thickness are respectively presented in Fig.5.

Figs.4 (a) and (b) show that when the rotational speed is 0, it is the Type 1 thrust bearing, namely hydro-static thrust bearing, which achieves the best load capacity and consumed least compressed air. Moreover, from Fig.4 (a), it can be seen that with the increase in groove depth, the load capacity decrease and the air consumption increase. This is because that with the grooves, the average air film thickness of herringbone grooved thrust bearings is larger than the one without the grooves. Thus leads to a lower load capacity and higher air consumption.

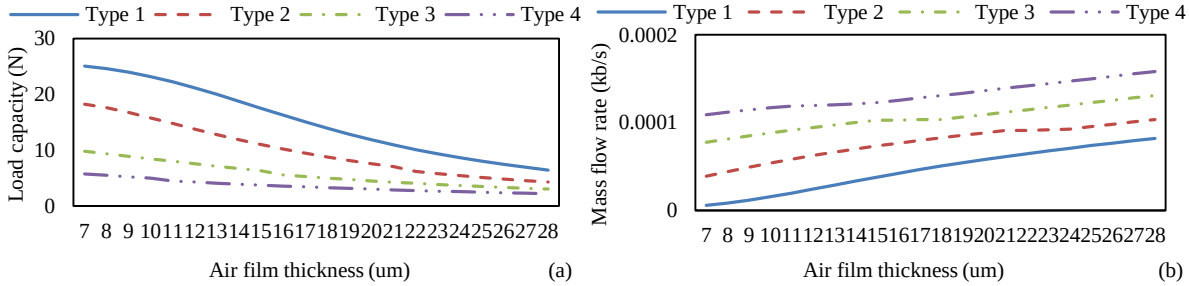

Figure 4. (a)The load capacity and (b) the mass flow rate of the 4 types of thrust air bearings versus the air film thickness when $\omega = 0$

From Fig.5 (a), it can be seen that at the speed of 300000 rpm and with a low air film thickness, Types 2 and 3 herringbone grooved bearings achieve a much higher load capacity than Type1, but Type 1 still achieve a higher load capacity than Type 4; with a high air film thickness, it is always Type 1 that achieves highest load capacity, but the difference with other 3 types of herringbone grooved thrust bearings are not obvious. This is because that the dynamic effect of the herringbone

grooved thrust bearings is proportional to the compressibility number Λ. With a low air film thickness and a high rotational speed, the compressibility number Λ can achieve a high value, which means a strong dynamic effect. As illustrated in Fig.5 (a), thrust bearings Types 2 and 3 have a low air film thickness and high rotating speed and the hydrodynamic effect caused by the grooves is strong enough to compensate the loss in load capacity caused by the increase of average air film thickness raised by the grooves; but with a high air film thickness, the compressibility number Λ decrease to a low value, and at this time the hydrodynamic effect caused by the groove is not enough to compensate the loss in load capacity caused by the grooves. Therefore, hydrostatic thrust bearing Type 1 achieves the highest load capacity. However, if the groove depth is very large, the bearing's performance will drop. This can be concluded from the Type 4 bearing, which has the largest air film thickness and thus always get a lower load capacity than the hydrostatic thrust bearing. From Fig.5 (b), it can be seen that the air consumption of the herringbone grooved thrust bearings is higher than that of non-grooved hydrostatic air bearings, and the air consumption increases with the groove depth.

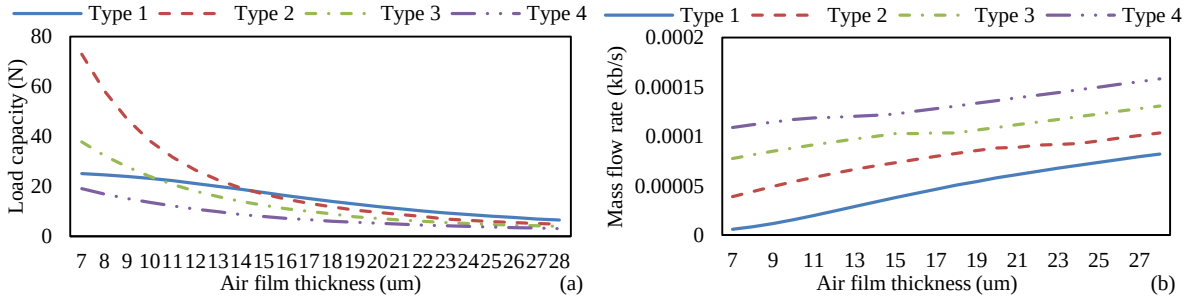

Figure 5.(a) The load capacity and (b) the mass flow rate of the 4 types of thrust air bearings versus the air film thickness when $\omega = 300{,}000$ rpm.

3.3. Analysis of dynamic response

Figs.6-7 give the dynamic step responses of the 4 types of thrust air bearings. The initial conditions used in all the cases are: $h_0 = 20\mu m$, $\dot{h}_o = 0$, $P_s = 6\ bar$, $w = 3N, dt = 10^{-5}$. The dynamic simulations take rotational speeds of $\omega_1 = 100{,}000$ rpm and $\omega_2 = 300{,}000$ rpm respectively.

From Fig.6, it can be seen that at $\omega_1 = 100{,}000$ rpm, the dynamic step responses of all the 4 types of thrust bearings are damped. However, from Fig.7, at speed $\omega_2 = 300{,}000$ rpm, thrust bearings Type 2 and Type 3 become undamped, while Types 1 and 4 remain damped. Therefore, it can be concluded herringbone grooved thrust bearings would lost the stability at high rotating speeds. Nevertheless, the stability of thrust bearings increases with the depth of the grooves; the same conclusion can be found in Reference [12]

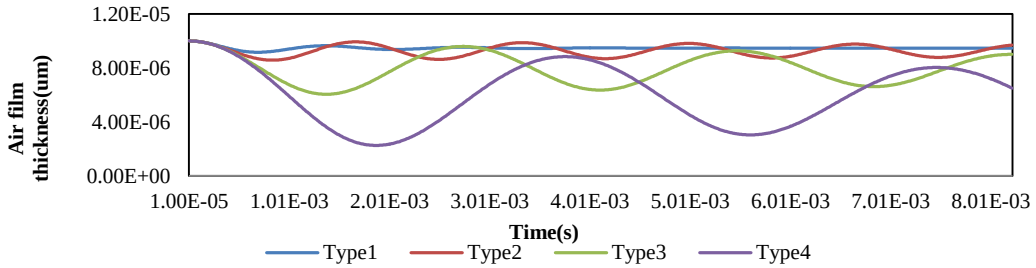

Figure 6. The dynamic step responses of the 4 types of thrust air bearings at a rotational speed of $\omega_1 = 100{,}000$ rpm.

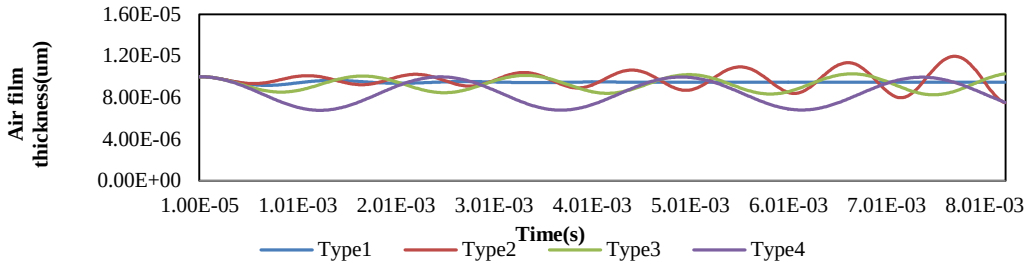

Figure 7. The dynamic step responses of the 4 types of thrust air bearings at a rotational speed of $\omega_2 = 300{,}000$ rpm.

4. Conclusions

In this paper, a numerical model of herringbone grooved thrust bearings, based on FDM and FVM, is presented and the load capacity, consumption of compressed air, and the dynamic response of herringbone grooved thrust bearings are investigated based on the proposed model. The influence of design parameters of the thrust bearings, including the air film thickness, rotating speed, groove depth and external load, on its characteristics have been investigated. Numerical results obtained show that hydrostatic thrust bearing can achieve a better load capacity and less air consumption than herringbone grooved thrust bearings at low compressibility number. Herringbone grooved thrust bearings can achieve a better load capacity but more air consumption than hydro-static thrust bearing at high compressibility number. In addition, herringbone grooved thrust bearings would lose the stability at high rotating speeds, and the stability of thrust bearings increases with the depth of the grooves. Same conclusions can be found in Reference [12].

Acknowledgments

The research is supported, in part, by European Horizon 2020 project 644971, Department for Transport T-TRIG 2017 project, and the scholarship from China Scholarship Council (CSC).

References

[1] Hashimoto, Hiromu, and Masayuki Ochiai. "Theoretical analysis and optimum design of high speed gas film thrust bearings." Journal of Advanced Mechanical Design, Systems, and Manufacturing 1.1 (2007): 102-112.
[2] Radu F A, Pop I S, Knabner P. Newton—Type Methods for the Mixed Finite Element Discretization of Some Degenerate Parabolic Equations[M]. Numerical mathematics and advanced applications. Springer Berlin Heidelberg, 2006: 1192-1200.
[3] Waumans, T., et al. "On the dynamic stability of high-speed gas bearings: stability study and experimental validation." Sustainable Construction and Design 2.2 (2011): 342.
[4] Wang, Nenzi, and Chinyuan Chang. "An application of Newton's method to the lubrication analysis of air-lubricated bearings." Tribology transactions 42.2 (1999): 419-424.
[5] Wang, Nenzi, Shih-Hung Chang, and Hua-Chih Huang. "Comparison of Iterative Methods for the Solution of Compressible-Fluid Reynolds Equation." Journal of Tribology 133.2 (2011): 021702.
[6] Wang, Nenzi, Shih-Hung Chang, and Hua-Chih Huang. "Stopping Criterion in Iterative Solution Methods for Reynolds Equations." Tribology Transactions 53.5 (2010): 739-747.
[7] Arghir, Mihai, Ahmad Alsayed, and Daniel Nicolas. "The finite volume solution of the Reynolds equation of lubrication with film discontinuities." International Journal of Mechanical Sciences 44.10 (2002): 2119-2132.
[8] Powell J W. Design of aerostatic bearings[J]. The Machinery Published Co. Ltd.1970.
[9] Neves MT, Schwarz VA, Menon GJ. Discharge coefficient influence on the performance of aerostatic journal bearings. Tribol Int 2010;43:746–51.
[10] Charki A, Bigaud D, Guérin F. Behavior analysis of machines and system air hemispherical spindles using finite element modeling. Ind Lubr Tribol 2013;65(4).

[11] Bonis M, Charki A. Modélisation des caractéristiques statiques et de la stabilité des paliers de butée aérostatiques par la méthode des éléments Finis[J]. Revue Européenne des Eléments, 2001, 10(6-7): 755-767.
[12] Theoretical analysis and optimum design of high speed air film thrust bearings (Application to optimum design problem).